A Section 508–conformant HTML version of this article is available at https://doi.org/10.1289/EHP10255.

Evaluation of Neurotoxicity in BALB/c Mice following Chronic Exposure to Polystyrene Microplastics

Haibo Jin,[1,2] Chen Yang,[3] Chengyue Jiang,[1,2] Luxi Li,[1,2] Mengge Pan,[1,2] Dongmei Li,[1,2] Xiaodong Han,[1,2] and Jie Ding[1,2]

[1]Immunology and Reproduction Biology Laboratory & State Key Laboratory of Analytical Chemistry for Life Science, Medical School, Nanjing University, Nanjing 210093, China
[2]Jiangsu Key Laboratory of Molecular Medicine, Nanjing University, Nanjing 210093, China
[3]State Key Laboratory of Analytical Chemistry for Life Science, School of Chemistry and Chemical Engineering, Nanjing University, Nanjing, Jiangsu, China

Background: The toxicity of microplastics (MPs) has attracted wide attention from researchers. Previous studies have indicated that MPs produce toxic effects on a variety of organs in aquatic organisms and mammals. However, the exact neurotoxicity of MPs in mammals is still unclear.

Objectives: We aimed to confirm the neurotoxicity of chronic exposure to polystyrene MPs (PS-MPs) at environmental pollution concentrations.

Methods: In the present study, mice were provided drinking water containing 100 μg/L and 1,000 μg/L PS-MPs with diameters of 0.5, 4, and 10 μm for 180 consecutive days. After the exposure period, the mice were anesthetized to gain brain tissues. The accumulation of PS-MPs in brain tissues, integrity of the blood–brain barrier, inflammation, and spine density were detected. We evaluated learning and memory ability by the Morris water maze and novel object recognition tests.

Results: We observed the accumulation of PS-MPs with various particle diameters (0.5, 4, and 10 μm) in the brains of exposed mice. Meanwhile, exposed mice also exhibited disruption of the blood–brain barrier, lower level of dendritic spine density, and an inflammatory response in the hippocampus. In addition, exposed mice exhibited cognitive and memory deficits compared with control mice as determined using the Morris water maze and novel object recognition tests, respectively. There was a concentration-dependent trend, but no particle size-dependent differences were seen in the neurotoxicity of MPs.

Conclusions: Collectively, our results suggested that PS-MPs exposure can lead to learning and memory dysfunctions and induce neurotoxic effects in mice, findings which have wide-ranging implications for the public regarding the potential risks of MPs. https://doi.org/10.1289/EHP10255

Introduction

Microplastics (MPs), defined as particles <5 mm in diameter, have been shown to be widespread in the marine environment.[1,2] Because of their small size, MPs cannot be completely degraded in aquatic organisms. Instead, they can pass through the food chain and eventually enter mammals, even humans.[3,4] Therefore, the toxicity of MPs has attracted extensive attention from researchers.

Many studies have demonstrated that MPs can produce certain toxic effects on the different organs of mammals and aquatic organisms, including the gastrointestinal tract,[5] kidney,[6] and gonads of mice[7] and liver of tadpoles and zebrafish.[8,9] Moreover, several studies have reported that MPs could accumulate in brain of freshwater fish red tilapia[10] and induce neurotoxicity in *Caenorhabditis elegans*[11] and the African catfish (*Clarias gariepinus*).[12] Strikingly, Chen et al. demonstrated that MPs exposure inhibited zebrafish larval locomotion, resulting in neurotoxicity.[13] In addition, Barboza et al. investigated neurotoxic effects of MPs and mercury in the European seabass (*Dicentrarchus labrax*).[14] The study indicated that MPs, mercury, and their mixtures caused neurotoxicity and oxidative stress and damage to the lipids. The decay of mercury in the water increased with MPs concentration. Nevertheless, the potential toxicity of MPs on the nervous system in mammals has been poorly reported. Previous studies have generally selected short-term acute exposure to explore the toxic effects of MPs on mammals, such as 28 d,[15] 40 d,[7] and 6 wk.[5] Few studies have investigated the toxic effects of long-term exposure. In this study, we chose 180-d exposure to evaluate the toxic effects of long-term MPs exposure on the nervous system.

A previous study demonstrated that polystyrene (PS) nanoplastics induced neurobehavioral alterations in adult zebrafish,[16] which suggested plastic particles can have toxic effects on animal behavior. There are many areas in the brain tissue responsible for different neural and behavioral functions; the present study is focused on hippocampus-mediated learning. The hippocampus is a significant part of the limbic system of the mammalian brain, and it is closely related to higher neural activities, such as learning and memory.[17] Numerous studies have confirmed that damage to the hippocampus of animals will decrease learning and memory ability significantly, as well as impair spatial memory and spatial navigation.[18–20] The hippocampal network is composed of many areas, such as the cornu ammonis 1 (CA1), cornu ammonis 3 (CA3), and dentate gyrus (DG). The Morris water maze (MWM) was first established in 1981 to measure hippocampal-dependent learning, including acquisition of spatial memory and long-term spatial memory.[21] Nowadays, the MWM test is a widely used method for assessing spatial learning and memory ability in mice. The MWM, which generally comprises a learning stage and testing stage, assesses the learning and memory of animals by analyzing data such as movement tracks and time spent searching for hidden platforms. The novel object recognition (NOR) test was introduced by Ennaceur and Delacour in 1988 to assess the ability of rats to recognize a novel object in a familiar environment.[22] Because mice have an innate preference for novelty, it has been successfully adapted for use in mice.[23] The NOR test is applied to assess short-term recognition memory of animals by recording and analyzing the exploring time spent with a familiar object and a novel one. In the present study,

Address correspondence to Jie Ding, Immunology and Reproduction Biology Laboratory & State Key Laboratory of Analytical Chemistry for Life Science, Medical School, Nanjing University, Nanjing, Jiangsu 210093, China. Email: djie@nju.edu.cn. And, Xiaodong Han, Immunology and Reproduction Biology Laboratory & State Key Laboratory of Analytical Chemistry for Life Science, Medical School, Nanjing University, Nanjing, Jiangsu 210093, China. Email: hanxd@nju.edu.cn

Supplemental Material is available online (https://doi.org/10.1289/EHP10255).

The authors declare they have no actual or potential competing financial interests.

Received 3 September 2021; Revised 7 September 2022; Accepted 13 September 2022; Published 12 October 2022; Corrected 13 December 2022.

Note to readers with disabilities: *EHP* strives to ensure that all journal content is accessible to all readers. However, some figures and Supplemental Material published in *EHP* articles may not conform to 508 standards due to the complexity of the information being presented. If you need assistance accessing journal content, please contact ehpsubmissions@niehs.nih.gov. Our staff will work with you to assess and meet your accessibility needs within 3 working days.

the MWM and NOR tests were applied to detect whether MPs treatment could induce cognitive impairment in mice.

The blood–brain barrier (BBB) refers to the barrier between the blood plasma and brain cells formed by the capillary wall of the brain and glial cells and the barrier between the blood plasma and cerebrospinal fluid formed by the choroid plexus, which might protect the brain tissue from harmful blood substances.[24–26] Previous studies have pointed out that environmental pollutants, such as heavy metals and fine particulate matter [PM $\leq$2.5 μm in aerodynamic diameter ($PM_{2.5}$)] could induce disruption of the BBB.[27–31] The breakdown of the BBB could result in inflammatory responses and neurodegeneration. It is still unclear whether MPs exposure could impair the integrity of the BBB structure.

Special note is needed that statistical units of MPs are diverse; for example, some research has used concentration units[32] and some quantity units.[33,34] In this study, we ensured consistency of concentration. The choice of concentrations in our study referred to reports and some previous articles.[5,32] Jin et al. used 100 and 1,000 μg/L 5-μm PS-MPs to investigate the impacts on the gut barrier.[5] Lu et al. used 100 and 1,000 μg/L PS-MPs with particle sizes of 0.5 and 50 μm to evaluate the effects on gut microbiota and hepatic lipid metabolism.[32] We chose two exposure concentrations (100 and 1,000 μg/L) of PS-MPs in this study because some natural polluted areas have reached this higher level.[4] Meanwhile, we considered that the concentration of exposure to mice in the laboratory can be higher, owing to the higher murine metabolic rate and stronger tolerance ability. Therefore, in summary, we used two different concentrations (100 and 1,000 μg/L) of 0.5-, 4-, and 10-μm PS-MPs to investigate whether concentration dependence existed.

In this study, we aimed to probe the toxicity of diverse particle diameters of PS-MPs on the nervous system in mice. Following chronic exposure to PS-MPs, the integrity of the BBB structure and the entrance of PS-MPs into brain tissue were investigated. In addition, we investigated whether memory ability and synaptic plasticity in mice were impaired by PS-MPs exposure. The findings of the present study may help us have a more comprehensive understanding of the neurotoxicity of MPs and serve as a wake-up call to raise awareness of environmental protection.

Materials and Methods

Characterization of PS-MPs

We obtained fluorescent PS-MPs (10 mg/mL) from the Tianjin Baseline ChromTech Research Center (Tianjin, China). Fluorescent MPs facilitate the detection of PS-MPs accumulation in tissue. We applied three sizes of PS-MPs—0.5-μm (7-3-0050), 4-μm (7-3-0400), and 10-μm (7-3-1000)—in this research. The shape and size of the MPs were measured by scanning electron microscopy (SEM; HITACHI). One microliter of PS-MPs (10 mg/mL) was suspended in 1 mL of double-distilled water (ddH_2O) and dried in critical point drying (K850; Quorum). The sample was attached to conductive carbon film double-sided adhesive and placed on the ion sputtering instrument sample table for about 30 s prior to imaging. The polymer type of MPs used in the study was detected by a laser confocal Raman spectrometer (Renishaw inVia-Reflex). The MPs solution was filtered through polycarbonate filters (GVS) to collect MPs, which were detected by Raman spectroscopy. The instrument was set as follows: laser with a 785-nm edge; grating of 1,200 L/mm (633/780); center of spectrum range of 1,150 cm^{-1}; exposure time of 1 s; laser power of 100%. Meanwhile, the zeta potential values of MPs were assessed by a zeta potentiometer (Malvern Panalytical Zetasizer Pro). The 1 μL of PS-MPs (10 mg/mL) was dispersed into 1 mL ultrapure water and added into the detection dish. After the electrode was cleaned, the MPs were put into the detection dish for zeta potential detection. The cycle was tested three times for each size of the PS-MPs, and the average value was calculated.

Animals and Treatment

Six-week-old specific pathogen-free (SPF) male BALB/c mice (weighing 19 ± 2 g) were obtained from the Medical School of Yangzhou University (Yangzhou, China). The mice were maintained at 20–22°C with 50%–60% relative humidity. All animals had free access to water and food and were kept on a 12 h:12 h light:dark cycle. The BALB/c mice were provided drinking water containing three sizes of PS-MPs for 180 consecutive days, and the water in the bottles was replaced every week. Before each water change, it was homogenized and mixed with ultrasonication to ensure the uniform distribution of MPs in the water. The mice were randomly assigned to seven groups ($n = 12$ for each group): *a*) control group (ddH_2O), *b*) 0.5 μm 100 μg/L–exposure group (1.437×10^9 particles/L), *c*) 0.5 μm 1,000 μg/L–exposure group (1.437×10^{10} particles/L), *d*) 4 μm 100 μg/L–exposure group (2.986×10^6 particles/L), *e*) 4 μm 1,000 μg/L–exposure group (2.986×10^7 particles/L), *f*) 10 μm 100 μg/L–exposure group (1.737×10^5 particles/L), and *g*) 10 μm 1,000 μg/L–exposure group (1.737×10^6 particles/L). The water intake, food intake, and body weight of the mice were measured once a week. Because the mice used in this study were from the same batch as those used in our previous study, refer to the previous article for the data regarding water intake, food intake, and body weight.[35] According to our previous measurements,[35] the water intake of each control mouse was about 3 mL/d. The total exposure to PS-MPs was therefore $\sim$0.3 μg/d per mouse and 3 μg/d per mouse at 100 and 1,000 μg/L, respectively. Following the exposure period, the mice were subjected to behavioral tests. We randomly selected 10 mice in each group for the behavioral tests. After the behavioral tests, the mice were deeply anesthetized with 2% sodium pentobarbital and the mouse brain, liver, and gastric tissues were harvested after cervical dislocation for the subsequent experiment. We randomly selected 3 mice in each group for ultrastructural analysis using electron microscopy, 3 mice in each group for biotin tracing, and 3 mice in each group for quantification of PS-MP accumulation in the brain and gastric tissues. After fluorescent imaging, the tissues were placed in paraformaldehyde for embedding. The hippocampal tissues of 6 mice in each group was taken out and quickly frozen in liquid nitrogen and stored at −80°C for RNA and protein extraction. All animal procedures were approved by the Animal Care and Use Committee of Nanjing University under animal protocol no. SYXK (Su) 2009-0017.

Morris Water Maze

The mice were given drinking water containing PS-MPs for 180 uninterrupted days. Following exposure, the mice were subjected to the MWM test to detect their spatial learning and memory ability. The day before the MWM test, the mice were acclimated to the water environment for 1 min. MWM testing was conducted in a round black pool with a diameter of 150 cm and a depth of 50 cm. The pool was arranged with drapes such that the mice being tested could not see the experimenter during testing. We placed high-contrast spatial cues about the pool to help the mice remember where the platform was located. A 10-cm diameter platform was placed in the center of one quadrant of the pool. The platform remained in the same position throughout the learning trials and visual cue tests and was removed from the pool during the probe test. Water temperature was maintained at $\sim$22°C. The mice were transferred directly from their housing facility to the behavior room, and once there, the mice were kept in an area where they could not see the pool or spatial cues. The mice were

allowed to adjust to the new environment for at least 30 min before testing. Day 1 was the visible platform phase; the platform was set 1 cm above the water level and marked with black tape so that the mice could locate the platform using a local visual stimulus rather than relying on spatial orientation to extra-maze cues. Days 2–5 comprised the hidden platform phase; we added additional water to the pool to submerge the platform to 1 cm below the surface. After the mouse was released, we retreated away from the pool to a constant position within the room, serving as an additional distal visual cue. The SMART digital tracking system (version 2.5; Panlab) simultaneously began recording the trial. During days 1–5, the maximum swim time was set to 90 s. If a mouse located the platform before 90 s had passed, it was immediately removed from the pool. If the platform was not located after 90 s of swimming, the mouse was gently guided to the platform and allowed to reorient to the distal visual cues for an additional 20 s before being removed from the pool. After removal from the pool, the mice were manually dried with a terrycloth towel and placed in a warming cage for at least 5 min before returning to the home cage. We tested all the mice in one quadrant, and then conducted the test in the second quadrant after 30 min. All testing was conducted at roughly the same time each day to minimize variability in performance due to time of day. Four quadrants were tested, and only the quadrant located farthest from the platform (the third quadrant) was analyzed. To examine spatial reference memory, a probe test was administered 24 h after the last training session. During the probe test (day 6), the platform was removed from the pool. The mice were placed into the third quadrant of the pool and allowed to swim freely for 90 s. After completion of the test, all tracks from all trials were analyzed for a number of behavioral parameters using SMART software (Panlab). Thigmotaxis is defined as the mice swimming in the outer 10% close to the walls, meaning the mice swim almost exclusively in the periphery. The rate of thigmotaxis was expressed as the ratio of the number of mice showing thigmotaxis to the total number of mice according to the swim path trajectories. The resultant behavioral data were statistically analyzed as described below.

Novel Object Recognition

Six-week-old BALB/c mice were provided drinking water containing PS-MPs for 180 consecutive days. After the exposure period, mice were subjected to the MWM test. The NOR test, which assesses short-term recognition memory, was performed 3 d after the MWM experiment. The experimental apparatus measured 40 cm × 40 cm × 40 cm. On the first and second days (training phase), two identical objects (5 cm × 5 cm × 5 cm) were placed in the experimental apparatus. Testing of object recognition memory occurred 24 h after training. The mice were tested on their preference for a new object compared with the old object. The objects were similar in size and darkness of color, but with slightly different shapes. Each mouse was placed on the side of the arena away from the object with its back to the object and allowed free exploration for 2 min. On each day of the experiment, the arena and objects were cleaned with 70% ethanol. All trials on both the training and testing days were videotaped and analyzed using the SMART digital tracking system. The total amount of time spent exploring the novel and familiar objects was recorded for each animal. A mouse was scored as exploring an object when it was directly sniffing or rubbing the object with its head or whiskers, biting, or licking the object. Looking without directly touching, sitting on, standing on, or sniffing the air above an object was not scored. The relative exploration time was recorded for each object. Data from training days (days 1–2) were expressed as a recognition score [time spent (s) investigating one object divided by the time spent (s) investigating both objects in total]. Data from the testing day were expressed as a novelty score [time spent (s) investigating novel object divided by the time spent (s) investigating both objects in total].

Tissue Accumulation of PS-MPs in Mice

Six-week-old BALB/c mice were provided drinking water containing PS-MPs for 180 consecutive days. After the behavioral test, the mice were deeply anesthetized with 2% sodium pentobarbital. The mouse brain and gastric tissues were collected after cervical dislocation. Gastric tissue was used as a positive control. Images were obtained of whole tissues using the biofluorescence imaging system LB 983 NightOWL II (BERTHOLD) equipped with a cooled slow-scan charged-coupled device camera. The 605-nm excitation filter and the 680-nm emission filter were selected to detect the accumulation of fluorescent PS-MPs in the tissues.

Hematoxylin-Eosin Staining

The brain tissues were fixed with 4% paraformaldehyde for 4 h, dehydrated in a graded ethanol series, and paraffin embedded. The embedded brain tissues were sectioned at 5 μm using a rotary microtome (RM2015; Leica). The slides were immersed in xylene for 10 min two times for dewaxing. Then the slides were dehydrated with an alcohol gradient concentration (100%, 95%, 90%, 70%, 50%, and 30% alcohol for 3 min per wash). The dehydrated slides were stained with hematoxylin for 45 s, washed with water, and rinsed with ammonia. The slides were then immersed in an alcoholic solution of varying concentrations (30%, 50%, 70%, and 90%) for 3 min. Subsequently, the slides were stained with 95% eosin for 5 min and soaked in 95% and 100% alcohol for 3 min. Finally, the slides were immersed in xylene and sealed with resin. The images were observed under a light microscope (Nikon) using the NewSmartv550D program.

Biotin-Tracing Assay

The mice were deeply anesthetized with 2% sodium pentobarbital, and cardiac perfusion was performed with phosphate-buffered saline (PBS) for 20 min. Then the mice were transcardially perfused with 20–25 mL Sulfo-NHS-LC-Biotin (0.5 mg/mL) (A8003; APExBIO) dissolved in PBS. The liver and brain tissues were collected and immersed in 4% paraformaldehyde for 4 h, followed by a solution of 30% sucrose overnight. The dehydrated liver and brain tissues were stored at −80°C. The tissues were embedded in OCT and cut into 10-μm–thick slides using a vibratome (CM1900; Leica). The frozen slices were dried at room temperature for 15 min. Slides were immersed in PBS for 10 min to remove the OCT. Triton (0.3%) was added to the glass slide for drilling for 10 min. Then the slides were washed with PBS for 10 min and sealed with a 3% bovine serum albumin (BSA) solution at 37°C for 30 min. The frozen sections were stained with streptavidin–Alexa Fluor 594 (Invitrogen) at 37°C for 1 h, and the nuclei were stained with 4′,6-diamidino-2-phenylindole (DAPI; Sigma-Aldrich) at 37°C for 15 min. The images were captured using a confocal fluorescence microscope FV10i microscope (Olympus).

Golgi–Cox Staining

After deeply anesthetizing the mice with 2% sodium pentobarbital, the mouse brain was harvested after cervical dislocation. The pia mater was removed carefully and ddH_2O was used to wash the blood from the surface. The dendritic spines in the hippocampus of the mice in the PS-MPs–exposed and control groups were

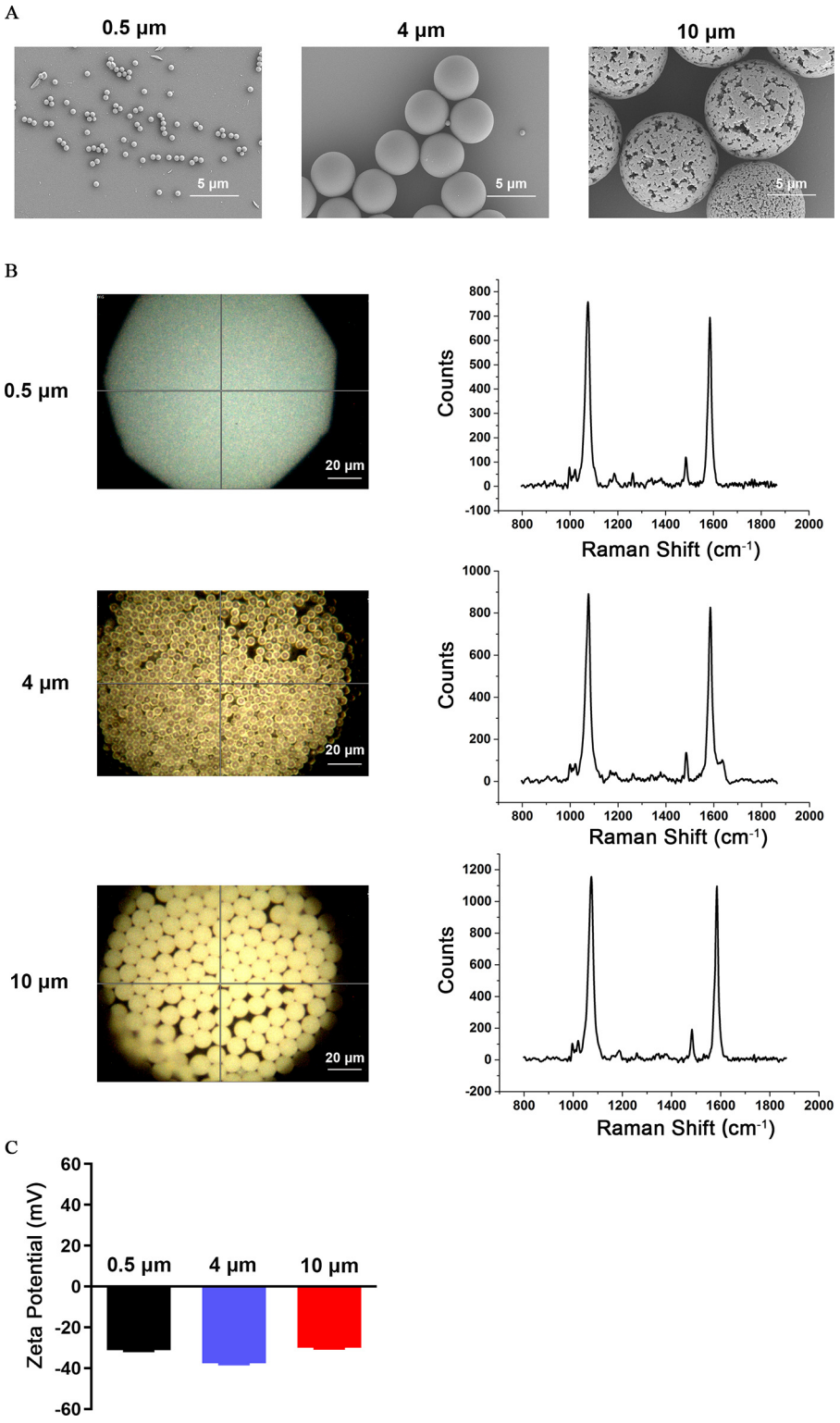

Figure 1. Characteristics of microplastics (MPs). (A) Scanning electron microscopy was used to detect the particle size and morphology of MPs (scale bar: 5 μm). (B) Qualitative analysis by Raman spectroscopy. The photomicrographs on the left are brightfield images of MPs taken under a laser confocal Raman spectrometer (scale bar: 20 μm). The graphs on the right show the Raman spectra of the MPs. (C) The zeta potentials of the three sizes of MPs were detected by a zeta potentiometer. Data are presented as the means ± SDs ($n = 3$/each size). The mean and SD summary data for quantification of (C) are shown in Table S3. Note: SD, standard deviation.

visualized by the Golgi–Cox staining procedure, according to the instruction manual in the FD Rapid Golgi Stain Kit manual (FD Neurotechnologies). The brains were immersed in impregnation solution (5% solution of potassium dichromate plus 5% solution of mercuric chloride) and stored at room temperature for 2 wk in the dark. The impregnation solution was replaced after the first 6 h of immersion or on the next day. The container was gently swirled side to side for a few seconds at least twice a week during the impregnation period. The tissue was then transferred into a 5% solution of potassium chromate and stored at room temperature in the dark for at least 72 h. The potassium chromate was replaced at least once after the first 24 h of

immersion or on the next day, and 100-μm sections were cut using a cryostat at −20°C. The slides were washed with ddH_2O twice for 5 min each and then incubated in a 20% ammonia solution for 10 min in the dark by gently shaking them. The slides were washed with ddH_2O twice for 5 min each and rinsed in a 1% sodium thiosulfate solution with gentle shaking it for 10 min. The sections were then washed with ddH_2O twice for 5 min each and dehydrated by processing through 50%, 75%, 95%, and 100% ethanol for 5 min each. The sections were defatted with xylene twice for 5 min each and coverslipped using mounting medium. The Golgi-stained sections were stored at room temperature protected from light. Images were obtained using a light microscope (Nikon). Dendrite branches in the hippocampus were counted using ImageJ software.[36]

RNA Extraction, Reverse Transcription, and Quantitative Real-Time Polymerase Chain Reaction

The hippocampus was soaked in 1 mL Trizol (Vazyme) and homogenized with an electric homogenizer. Two hundred microliters of chloroform was added to the lysate, and it was fully oscillated on an oscillator for 30 s and allowed to stand for 10 min. After centrifugation at 12,000 rpm for 10 min at 4°C, the supernatant was absorbed into a clean enzyme-free eppendorf (EP) tube, into which 100% isopropyl alcohol of equal volume was added. The liquid was incubated at room temperature for 10 min, and we mixed it by inversion five times during the incubation. After centrifugation at 12,000 rpm at 4°C for 10 min, we discarded the supernatant and washed the pellet with 1 mL of 75% ethanol solution. The precipitate was suspended as much as possible and then centrifuged at 7,500 × *g* at 4°C for 5 min. The supernatant was discarded, and the EP tube was dried at room temperature for 8 min. Enzyme-free water was added to the EP tube, and the RNA concentration was detected after incubation in a metal bath at 60°C for 10 min. The complement DNA (cDNA) was generated by HiScript Q RT SuperMix (R122-01; Vazyme). The reaction conditions were 50°C for 15 min and 85°C for 2 min. Quantitative real-time polymerase chain reaction (qRT-PCR) was performed using ChamQ Universal SYBR qPCR Master Mix (Q711-02; Vazyme) and an RT-PCR System (ABI Viia 7). The reaction conditions were 30 s at 95°C, followed by 45 cycles of denaturation at 95°C for 10 s, annealing at 60°C for 30 s, and extension at 72°C for 15 s. The primer sequences (Tsingke) applied in this research are shown in Table S1. The relative quantification values of the target genes were measured by the $2^{-\Delta\Delta Ct}$ method, and glyceraldehyde 3-phosphate dehydrogenase (GAPDH) was used as an internal reference.[37]

Protein Extraction and Western Blotting

The hippocampus tissues were minced with scissors and homogenized with an electric homogenizer. Proteins were purified from the brain tissues by using radioimmunoprecipitation assay (RIPA) buffer (P0013C; Beyotime). The tissues were placed in RIPA buffer containing protease inhibitor cocktail (HY-K0010; MedChemExpress) and lysed on ice for 30 min. The centrifuge (Heraeus Fresco 17; Thermo) was precooled to 4°C in advance. The whole lysates were then centrifuged at 12,000 × *g* for 30 min to remove debris. The protein concentration in the supernatant was determined using bicinchoninic acid protein quantification kit (E112-02; Vazyme) and measured at a wavelength of 562 nm in a microplate reader (Molecular Devices M3). The loading buffer was added to the protein extract and heated at 100°C for 10 min. Approximately 30 μg of proteins from each sample were separated on a 10% sodium dodecyl sulfate–polyacrylamide gel electrophoresis gel and then electrophoretically transferred onto polyvinylidene fluoride (PVDF) membranes

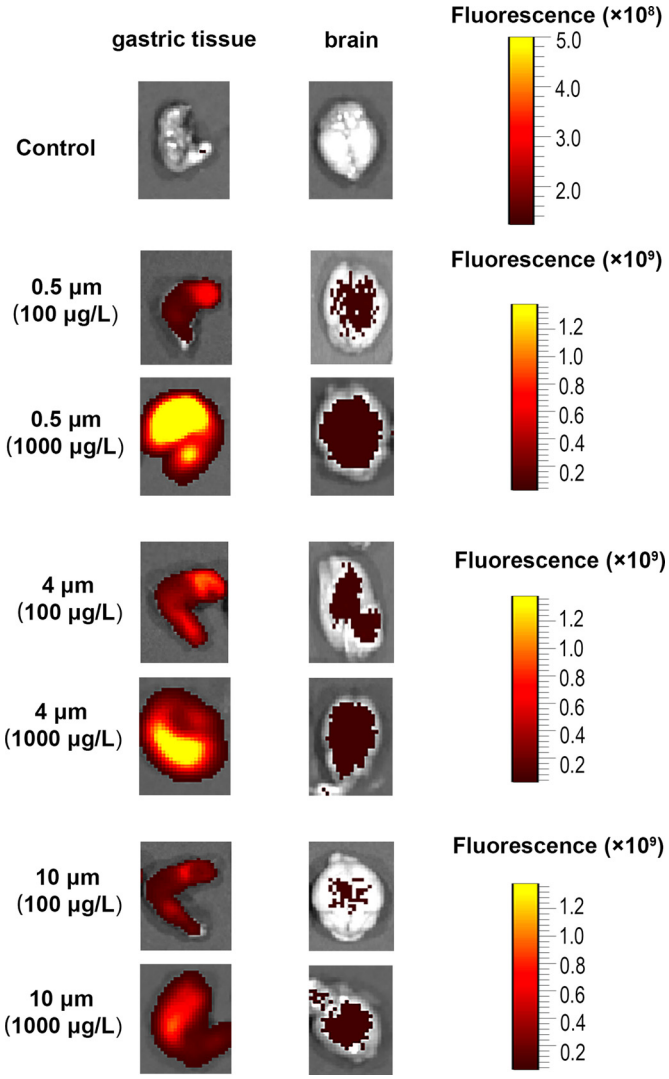

Figure 2. Biodistribution of various diameters of polystyrene microplastics (PS-MPs) in different tissues of mice. Mice were provided drinking water containing three sizes of fluorescent PS-MPs for 180 consecutive days. Fluorescence photomicrographs of excised brain tissues and gastric tissues were evaluated ($N = 3$ mice/group), the images display representative animals in each group. Images of other mice are shown in Figure S1. The colors in the photomicrographs indicate the fluorescence of the PS-MPs in the tissues.

(Millipore). The membranes were incubated at 37°C for 1 h in blocking buffer (PBS, 0.1% Tween-20, 5% BSA). The primary antibodies mouse anti-GAPDH, rabbit anti-PSD95, rabbit anti-synapsin 1, and rabbit anti-synaptophysin (all from Proteintech) were used to incubate the transferred blots overnight at 4°C. Detailed information of the primary antibodies is displayed in Table S2. After six washes in PBS/Tween (PBS, 0.1% Tween-20), the membranes were incubated with the secondary antibodies horseradish peroxidase–conjugated goat anti-rabbit/mouse IgG (BA1039/BA1038; Boster) (dilution 1:5,000) at 37°C for 1 h. Immunoreactive protein bands were detected using enhanced chemiluminescence solution (Millipore) by an Odyssey Scanning System (LI-COR). Band densitometry was quantified using ImageJ software. In addition, GAPDH was chosen as the internal control.

Transmission Electron Microscopy

Transmission electron microscopy was applied to detect the ultrastructure of the BBB. Fresh brain tissues were placed in 3%

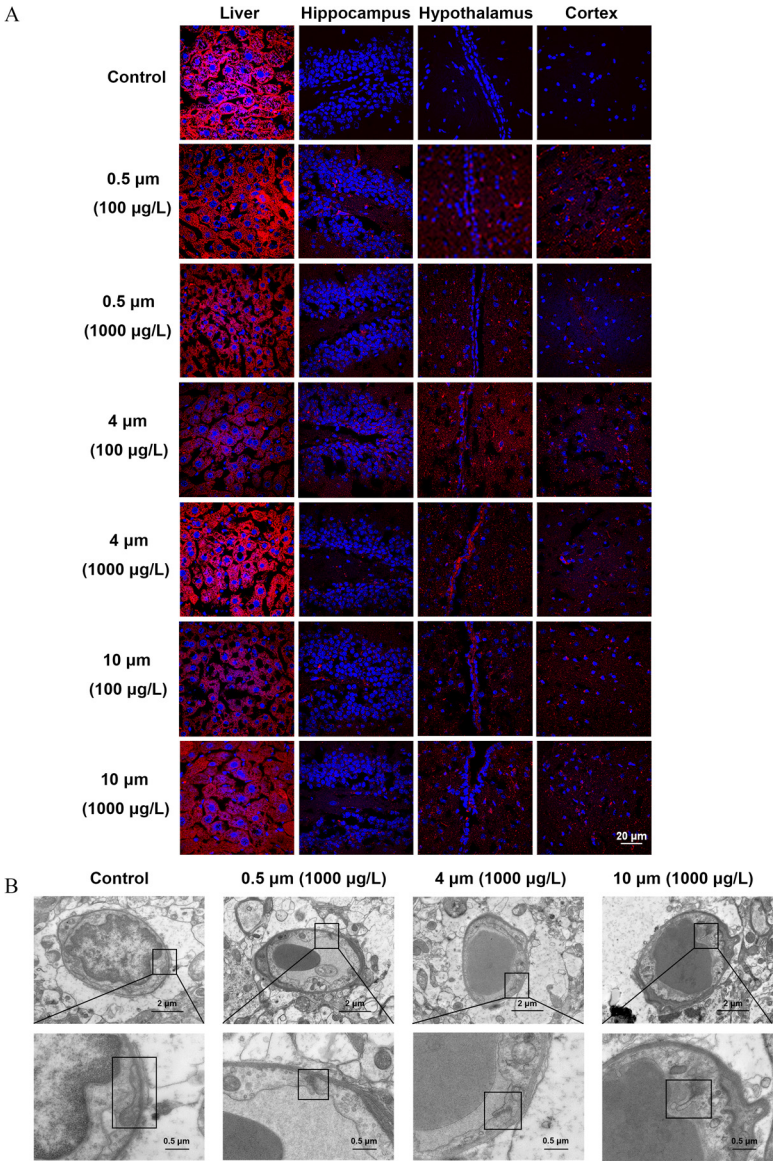

Figure 3. The integrity of the blood–brain barrier (BBB) in mice treated with polystyrene microplastics (PS-MPs). Mice were exposed to three sizes of fluorescent PS-MPs dissolved in water for 180 days. (A) BBB integrity was detected by biotin tracer experiments. The liver and brain tissues were collected and immersed in paraformaldehyde, followed by a solution of 30% sucrose overnight. The tissues were embedded in OCT and cut into sections. The sections were stained with biotin (red) and DAPI (blue). The existence of biotin in brain tissues was examined by immunofluorescence microscopy ($N = 3$ mice/group, $n = 3$ slides/mice). The biotin signal of the liver parenchyma was used as a positive control. Images of other mice are shown in Figure S2. (B) PS-MPs–induced ultrastructural changes in the BBB were detected by a transmission electron microscope. Upper images display the ultrastructure of BBB. Lower images refer to the magnified boxed areas. These are representative images ($N = 3$ mice/group). Images of other mice are shown in Figure S3. Note: DAPI, 4′,6-diamidino-2-phenylindole.

glutaraldehyde (G7526; Sigma-Aldrich) for 2 h followed by 2% osmium tetroxide (19100; Electron Microscopy Sciences) for 3 h. The tissues were dehydrated and embedded in spurr resin, then cut into 70-nm ultrathin sections by ultratome (PowerTome-XL; RMC). The sections were stained with 3% uranyl acetate (22400; Electron Microscopy Sciences) and 2% lead citrate (17800; Electron Microscopy Sciences). The sections were examined using a JEM-1200 EX II TEM (JEOL) operated at 80 kV. We captured the imaging of the ultrastructure of the BBB using a Hitachi transmission electron microscopy (TEM) system.

Statistical Analyses

The statistical analysis was based on SPSS 18.0 (IBM). GraphPad Prism Software (version 8.0.1) was used to plot the data. The values are presented as means ± standard deviations. For the MWM tests, only the time the mice took moving from the third quadrant to the target platform during the learning trials (days 1–5) was analyzed. The thigmotaxis of mice on days 1–5 were analyzed. The thigmotaxis was the ratio of the number of mice showing thigmotaxis of four trials to the total number of mice according to the swim path trajectories of four trials in every day. During the probe test (day 6), the mice were placed in the third quadrant of the pool. The number of times the mice passed the target platform on the sixth day were measured. The percentage of time the mice took in the quadrant where the target platform was placed on the sixth day was detected. All statistical tests were two sided, and the data were considered significantly different when the p-value was <0.05. Differences between groups were detected by one-way analysis of variance (ANOVA) followed by Dunnett's multiple comparison tests.

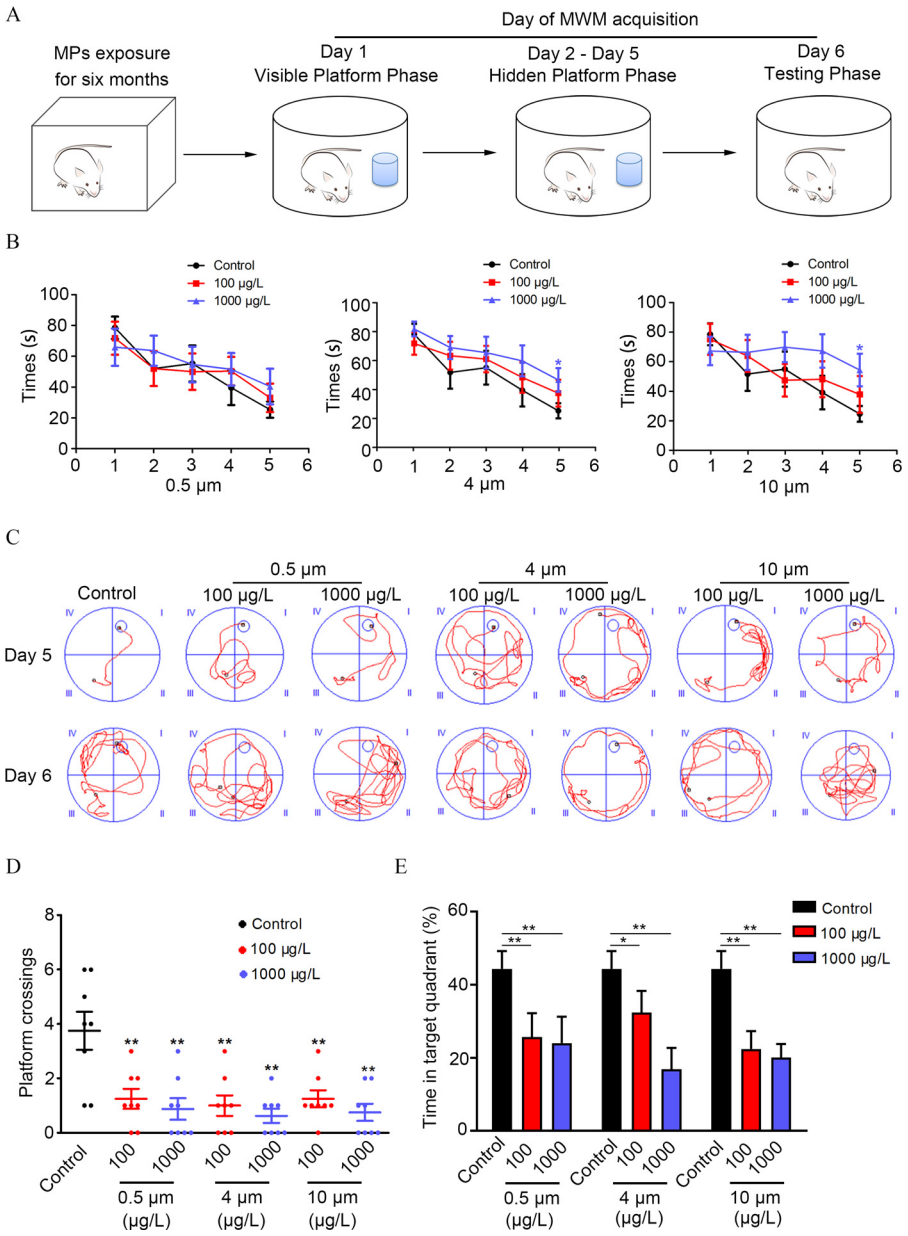

Figure 4. Spatial learning and memory ability in mice treated with polystyrene microplastics (PS-MPs). Mice were tested in a Morris water maze (MWM) experiment following treatment with PS-MPs for 180 days. (A) The experimental design of the MWM test is displayed. Day 1 was the visible platform phase, and the platform was set 1 cm above the water level. Days 2–5 comprised the hidden platform phase, and additional water was added to the pool to submerge the platform to 1 cm below the surface. Day 6 was the testing phase, and the platform was removed from the pool. The SMART digital tracking system (version 2.5; Panlab) was used to record the trial. The mean and SD summary data for quantification are shown in Table S3. *p*-Values for all comparisons are reported in Table S4. (B) The time it took the mice to move from the third quadrant to the target platform during the learning trials (days 1–5) was measured. The mean and SD summary data for quantification are shown in Table S3. *p*-Values for all comparisons are reported in Table S4. (C) Representative swimming routes of mice from the third quadrant to the target platform on the fifth and sixth days are shown. (D) The number of times the mice passed the target platform on sixth day are displayed. The mean and SD summary data for quantification are shown in Table S3. *p*-Values for all comparisons are reported in Table S4. (E) On the sixth day, the percentage of time the mice took in the quadrant where the target platform was placed was detected. Data are presented as the means ± SD ($N = 10$ mice/per group). The mean and SD summary data for quantification are shown in Table S3. *p*-Values for all comparisons are reported in Table S4. $^{*}p < 0.05$; $^{**}p < 0.01$ vs. control, as determined by one-way ANOVA followed by Dunnett's multiple comparison tests. Note: ANOVA, analysis of variance; SD, standard deviation.

Results

Characterization of MPs

We obtained fluorescent PS-MPs in three sizes: 0.5, 4, and 10 μm. The shape and size of the MPs were measured by SEM. We found that the MPs used in this study appeared regular-spherical, and the size met our requirements (Figure 1A). The polymer type of MPs was PS according to the Raman spectra (Figure 1B). We also detected the zeta potential values of MPs. The zeta potential value represents the surface charge of the MPs, which is important for its toxicity. The zeta potential value of PS-MPs with the three particle sizes ranged from −30 to −40 mV (Figure 1C).

Accumulation of PS-MPs in the Brains of Mice

Six-week-old BALB/c mice were provided drinking water containing three sizes of fluorescent PS-MPs for 180 consecutive

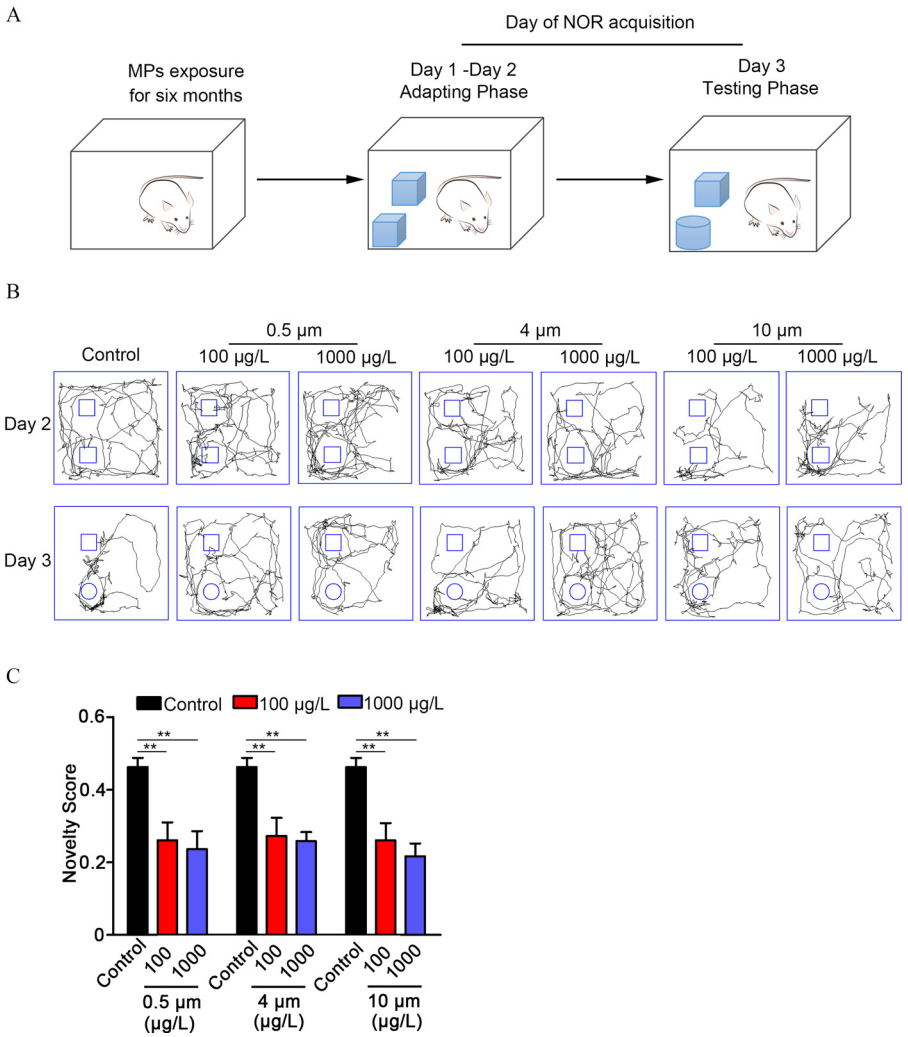

Figure 5. Short-term recognition memory function in mice treated with polystyrene microplastics (PS-MPs). Three days after the Morris water maze (MWM) experiment, a novel object recognition (NOR) experiment was performed. (A) The experimental design of the NOR test is displayed. On the first and second days (training phase), two identical objects were placed in the experimental apparatus. Testing of object recognition memory (the third day) occurred 24 h after training. Mice were tested on their preference for a new object compared with the old object. All trials on both the training and testing days were videotaped and analyzed by the SMART digital tracking system (version 2.5; Panlab). (B) The walking routes of mice on the second and third days are shown. The pictures display representative animals in each group. (C) The novelty scores [time spent (s) investigating novel object divided by the time spent (s) investigating both objects in total] of mice were examined. The results are expressed as means ± SDs ($N = 10$ mice/per group). The mean and SD summary data for quantification are shown in Table S3. p-Values for all comparisons are reported in Table S4. $^{**}p < 0.01$ vs. control, as detected by one-way ANOVA followed by Dunnett's multiple comparison tests. Note: ANOVA, analysis of variance; SD, standard deviation.

days, after which fluorescence images of the brain and gastric tissues of the mice were measured using biofluorescence imaging. Gastric tissue was used as a positive control. Fluorescent PS-MPs were found in the brain and gastric tissues (Figure 2; Figure S1).

The Integrity of BBB in PS-MPs Treated Mice

A biotin tracer assay was widely used to qualitatively detect the integrity of the BBB structure. Biotin signals were observed in the parenchyma of the liver in both control and PS-MPs–exposed mice because of the fenestrated vasculature.[38] However, biotin signals were displayed in the hippocampus, hypothalamus, and cortex in the different sizes of PS-MPs–exposure groups but not the control group (Figure 3A; Figure S2). Three mice were evaluated in each group. They all displayed the described phenotype. Meanwhile, the ultrastructure of the BBB was evaluated using TEM. The tight junction structure between adjacent endothelial cells presented a relatively complete band in the control group. In contrast, the tight junction structure became shorter and thinner in the experimental groups (Figure 3B; Figure S3). Three mice were evaluated in each group. They all displayed the described phenotype.

Learning and Memory Function in PS-MPs–Treated Mice

The experimental design of the MWM test is displayed in Figure 4A. There were no significant differences between control and PS-MPs–exposed mice in their ability to locate the target platform during the training stage on days 1–4. Mice exposed to 4- and 10-μm PS-MPs at a dose of 1,000 μg/L took a longer time to find the hidden platform than the control mice on day 5 (Figure 4B). The time for the mice to find the hidden platform could reflect the learning and memory function of mice. A shorter time for the mice to find the platform means better learning and memory ability in mice. The average swim speed of mice on days 1–5 was not significantly different between PS-MPs–treated and -untreated mice (Figure S4). There was no difference in the thigmotaxis among groups. However, for each group, the percentage

of mice exhibiting the thigmotaxis decreased almost every day (Table S5). For each group, the total path length to find the hidden platform of mice also decreased almost every day. The total path length to find the hidden platform of mice exposed to 4-μm PS-MPs at a dose of 1,000 μg/L was significantly lower compared with the control mice on day 5 (Figure S5). Compared with the control group, mice in the PS-MPs–treated groups crossed the missing platform significantly less frequently within 90 s during the testing phase on day 6 (Figure 4C,D). Meanwhile, the time that PS-MPs–exposed mice stayed in the quadrant of the missing platform was substantially less than that of the control group, and there was no significant difference among different diameters of PS-MPs (Figure 4E). The more time the mice crossed the missing platform, the longer they stayed in the quadrant where the platform was located, suggesting that the mice had a memory of the location of the platform.

The experimental design of the NOR test is displayed in Figure 5A. We examined the recognition scores in days 1–2. The recognition scores of most mice were around 0.5, indicating that the time spent exploring two identical objects was essentially the same and that there was no preference (Figure S6). On the testing day, the total distance moved and the average movement speed of the mice tended to be less in mice exposed to PS-MPs, and there was a significant difference in distance moved in the 1,000 μg/L 10-μm PS-MPs–exposure group (Figure 5B; Figure S7). Because of their innate preference for novelty, if a mouse recognizes a familiar object, it will spend most of its time at the novel object. The novelty scores were applied to assess short-term recognition memory of mice. Results demonstrated that the novelty scores were greatly lower in the PS-MPs–exposure groups in comparison with the control group (Figure 5C).

Nucleolar Characterization and the mRNA Levels of Proapoptotic Genes in the Hippocampus of PS-MPs Treated Mice

Hematoxylin-eosin (H&E) staining of the brain showed deeper nucleolar staining of neurons in the CA3 and DG regions of the hippocampus in mice exposed to PS-MPs compared with control mice (Figure 6). Lower neuronal cell numbers in the DG region were observed in 1,000 μg/L 0.5-μm PS-MPs and 100 μg/L 4-μm PS-MPs–exposure group (Figure S8). No differences in cell numbers in the CA1 and CA3 region were observed. Meanwhile, the mRNA levels of *caspase 3* were significantly higher in the hippocampus in mice exposed to PS-MPs compared with control mice (Figure S9A). Moreover, the *Bax/Bcl-2* mRNA ratio was markedly higher (Figure S9B).

Density of Dendritic Spines and Expression of Proteins Related to Synaptogenesis in the Hippocampus of PS-MPs–Treated Mice

Dendritic spines, which are located on the dendrites of neurons that form synapses, are closely related to learning and memory. Golgi–Cox staining was widely used to quantitatively analyze dendritic spines. Mice exposed to PS-MPs had fewer spines located in the CA1 region of the hippocampus (Figure 7A,B). Furthermore, the expression of synapsin 1, synaptophysin, and PSD 95 protein was lower in a concentration-dependent manner in the hippocampus of PS-MPs–exposed mice compared with control mice (Figure 7C; Figure S10). Meanwhile, the levels of *Ncam*, *Syt 4*, *Syt 1*, *Bdnf*, and *Gap43*, which are involved in the synaptogenesis of neurons in hippocampus tissues, were evaluated. The qRT-PCR results showed that mice exposed to PS-MPs had lower mRNA levels of *Bdnf* and *Syt 1* in the hippocampus (Figure 7D,E). However, there were no significant differences between control and PS-MPs–exposed mice in mRNA levels of *Gap43* and *Syt 4*. The mRNA level of *Ncam* was markedly lower in the 100 μg/L 10-μm PS-MPs–exposure group (Figure S11).

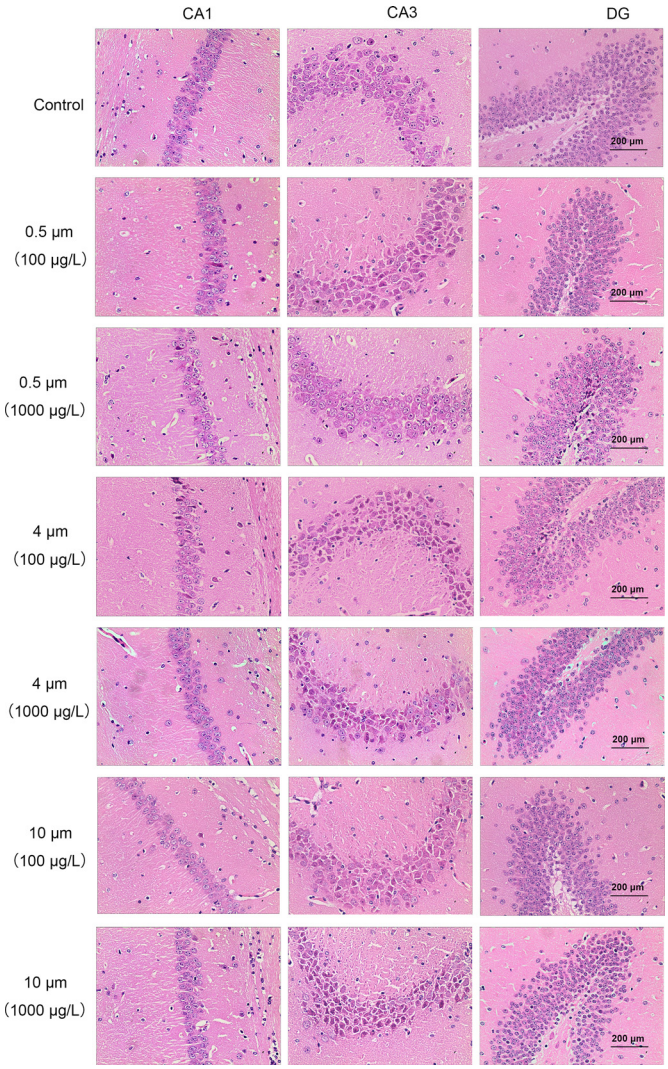

Figure 6. Hematoxylin-eosin (H&E) staining in brain sections and expression of proapoptotic proteins in the hippocampus of mice treated with polystyrene microplastics (PS-MPs). H&E staining was used to stain hippocampal CA1, CA3, and DG regions. Hematoxylin stained the cell nuclei blue, and eosin stained the extracellular matrix and cytoplasm pink (scale bar: 30 μm) ($N = 3$ mice/group, $n = 3$ slides/mice). Note: CA1, cornu ammonis 1; CA3, cornu ammonis 3; DG, dentate gyrus.

Expression of Proteins Related to Inflammation in the Hippocampus of PS-MPs–Treated Mice

The levels of inflammation-related genes, such as tumor necrosis factor alpha (*Tnf*-α), interleukin-1β (*Il*-1β), interleukin-6 (*Il-6*), chemokine (*C-X-C motif*) ligand 10 (*Cxcl10*), and monocyte chemoattractant protein-1 (*Mcp-1*) in the hippocampus were measured. The gene expression levels of *Tnf*-α, *Il*-1β, *Il-6*, *Cxcl10*, and *Mcp-1* were markedly higher in the PS-MPs–exposed mice compared with the control group (Figure 8). In addition, the immunofluorescence staining of hippocampus tissues displayed higher expression of Mcp-1 and Tnf-α protein in mouse brain following the treatment with PS-MPs (Figure S12).

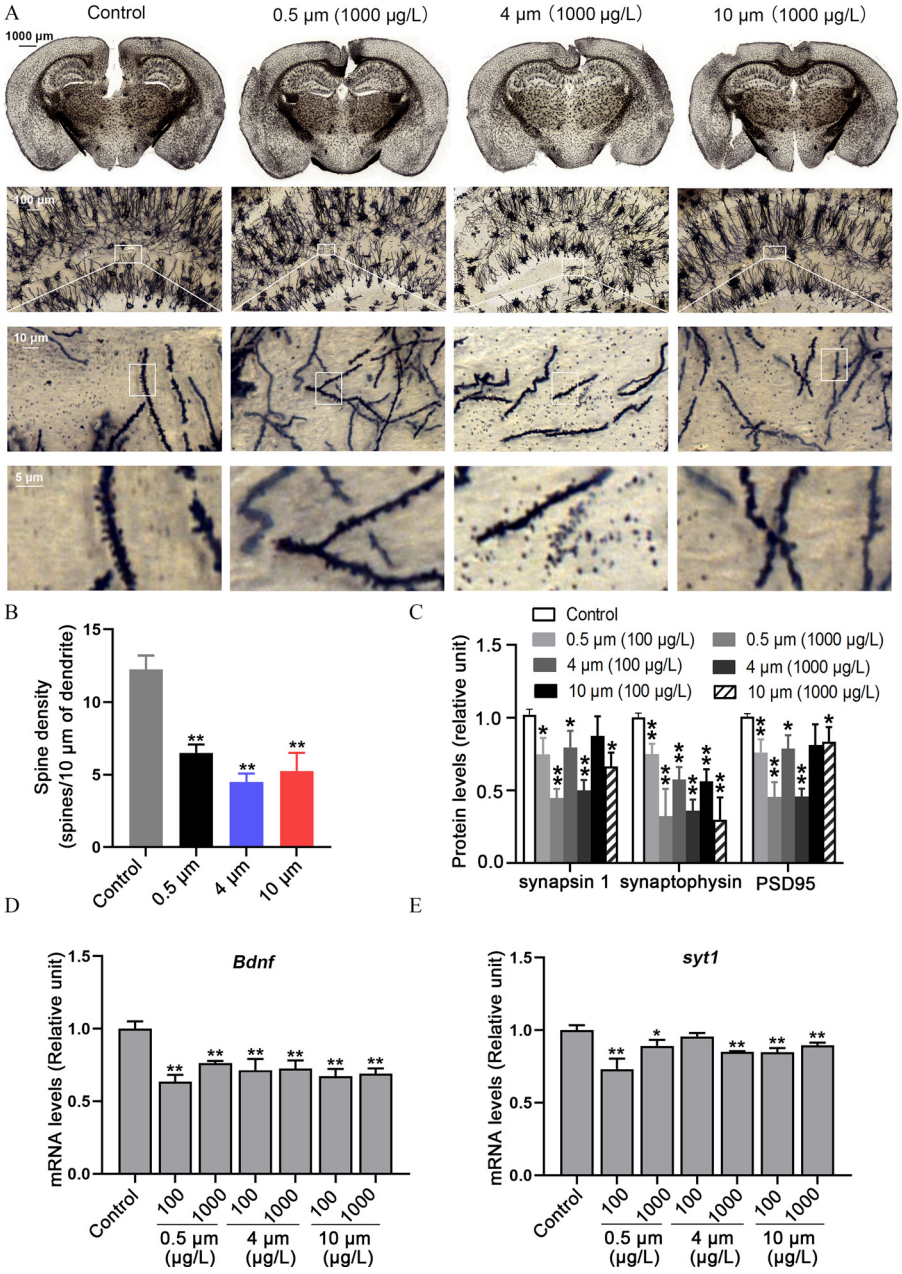

Figure 7. The density of dendritic spines and expression of proteins related to synaptogenesis in the hippocampus of polystyrene microplastics (PS-MPs)–treated mice. (A) Golgi–Cox staining examined the effect of PS-MPs on the density of dendritic spines in the hippocampus. (B) The number of spines were counted. The mean and SD summary data for quantification are shown in Table S3. *p*-Values for all comparisons are reported in Table S4. (C) The expression of synapsin 1, synaptophysin, and PSD 95 protein in the hippocampus was measured via western blotting. The western blotting results are shown in Figure S10. Quantification of western blotting evaluating synapsin 1, synaptophysin, and PSD95 protein in the hippocampus of PS-MPs treated mice. The expression levels were quantified with ImageJ[36] ($n = 3$). Data are presented as the means ± SDs. The mean and SD summary data for quantification are shown in Table S3. *p*-Values for all comparisons are reported in Table S4. *, $p < 0.05$; **, $p < 0.01$ compared with the control group, as determined by one-way ANOVA with Dunnett's multiple comparison test. (D,E) The mRNA levels of *Bdnf* and *syt 1* in the hippocampus were tested with qRT-PCR by normalizing to *Gapdh*. The results are expressed as means ± SDs ($n = 3$, $N = 3$ mice/group). The mean and SD summary data for quantification are shown in Table S3. *p*-Values for all comparisons are reported in Table S4. *$p < 0.05$; **$p < 0.01$ compared with the control group, as determined by one-way ANOVA followed by Dunnett's multiple comparison tests. Note: ANOVA, analysis of variance; Bdnf, brain-derived neurotrophic factor; Gapdh, glyceraldehyde 3-phosphate dehydrogenase; qRT-PCT, quantitative real-time polymerase chain reaction; SD, standard deviation; syt1, synaptotagmin-1.

Discussion

At present, owing to the widespread use of plastic products, plastic pollution is becoming increasingly serious.[39,40] Therefore, the potential toxicity risks MPs pose to aquatic organisms and mammals have raised extensive concern from researchers.[41] Previous studies have demonstrated that MPs could do harm to the liver,[8,32] gut,[32] lung,[42] and reproductive system[43,44] in a variety of experimental animal models. Nevertheless, little is known about the neurotoxicity of MPs exposure in mammals. To simulate environmental exposure to MPs in humans, this study evaluated the toxic hazards of chronic MPs treatment on the brains of mice.

Some researchers have pointed out that MPs induce neurotoxicity in aquatic organisms. For example, Barboza et al. showed that MPs caused neurotoxicity through acetylcholinesterase inhibition

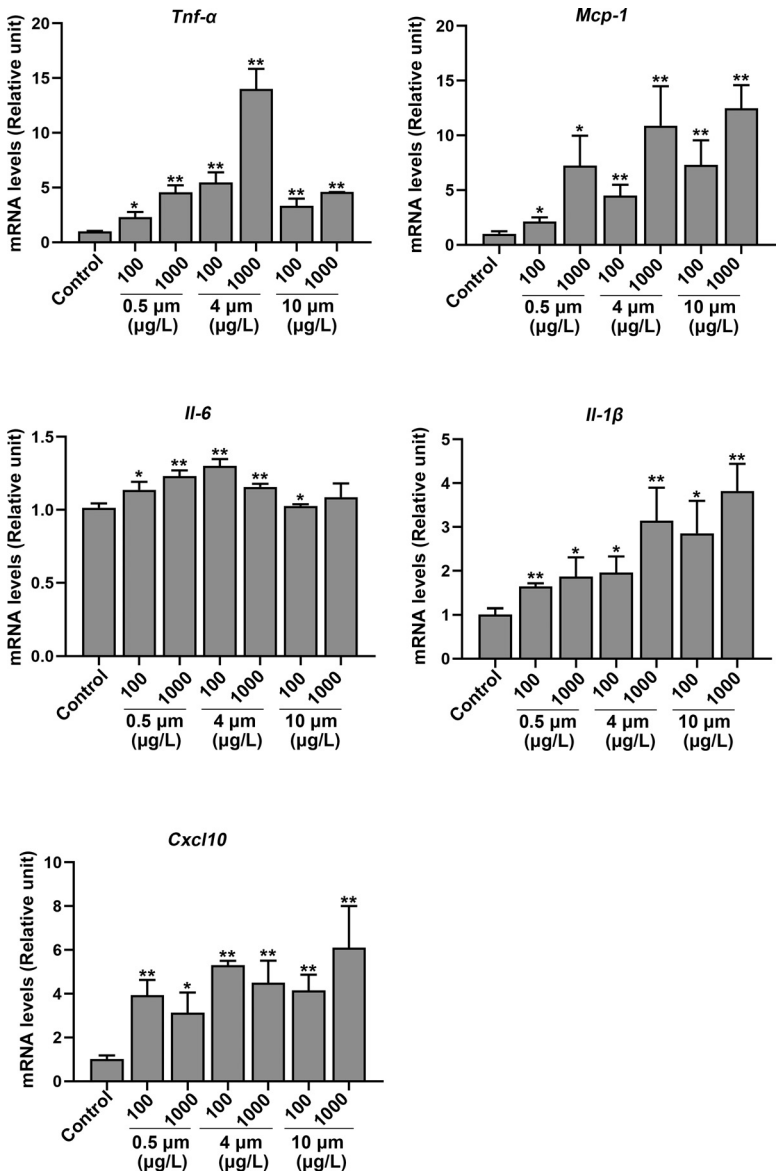

Figure 8. mRNA expression of proteins related to inflammation in the hippocampus of polystyrene microplastics (PS-MPs)–treated mice. The levels of tumor necrosis factor alpha (*Tnf*-α), interleukin-1β (*Il*-1β), interleukin-6 (*Il-6*), chemokine (*C-X-C motif*) ligand 10 (*Cxcl10*), and monocyte chemoattractant protein-1 (*Mcp-1*) in the hippocampus were measured via qRT-PCR. Data are expressed as the means ± SDs for three independent experiments ($N = 3$ mice/group). The mean and SD summary data for quantification are shown in Table S3. *p*-Values for all comparisons are reported in Table S4. $^{*}p < 0.05$; $^{**}p < 0.01$ vs. control, as detected by one-way ANOVA followed by Dunnett's multiple comparison tests. Note: ANOVA, analysis of variance; qRT-PCT, quantitative real-time polymerase chain reaction; SD, standard deviation.

and an increase in lipid oxidation in the brains of European seabass.[14] Tang et al. demonstrated that combined exposure to bisphenol A and MPs led to a higher level in pivotal neurotransmitters, inducing neurotoxicity in *Tegillarca granosa*.[45] Sun et al. confirmed that MPs exposure apparently inhibited the average speed and distance traveled by aquatic organisms, resulting in a neurotoxic response.[46] In the present study, we discovered that fluorescent PS-MPs were found in the brain, indicating that PS-MPs with various sizes in diameter could enter and accumulate in the brains of mice. The results of the MWM and NOR tests suggest learning and cognitive impairment in mice exposed to PS-MPs compared with control mice. Biotin was transcardially perfused into the blood circulation of mice. Biotin signaling does not occur in brain tissue with intact BBB. However, biotin signals were found in the hippocampus, hypothalamus, and cortex in the PS-MPs–exposure groups. The tight junction structure in PS-MPs–exposure groups was shorter and thinner than that in the control mice, consistent with the destruction of the BBB of PS-MPs exposed mice. The BBB plays a critical role in preventing harmful substances from entering brain tissue and in maintaining homeostasis.[47,48] Disruption of the BBB could lead to inflammation and neurodegenerative diseases.[49] As expected, the mice exposed to PS-MPs had higher mRNA levels of the inflammatory cytokines *Tnf*-α, *Il*-1β, *Il-6*, *Cxcl10*, and *Mcp-1*. Moreover, the MWM and NOR behavioral tests were performed to assess the adverse consequences of chronic PS-MPs treatment on the cognitive and memory function of mice.[50,51] Spatial learning and memory ability was assessed in the MWM test. The results of the MWM test suggested that mice in the PS-MPs–treated groups crossed the missing platform significantly less frequently during the testing phase compared with the control group. The time that the PS-MPs–exposed mice stayed in the quadrant of the missing platform was substantially less than that of the control group. A higher percentage

of time spent in the platform quadrant is interpreted as a higher level of memory retention. NOR testing was used to assess short-term recognition memory. The results of NOR testing demonstrated that the novelty score was greatly lower in the PS-MPs–exposure groups in comparison with the control group. Generally, NOR novelty scores should be >0.5 (the no-preference score) to show that the mice had a preference for the novel object, implying memory of the previously explored object. In our results, we discovered that novelty scores of some mice in the control group were <0.5. We suspect that there are two reasons for this. On the one hand, this may be due to the fact that the time we measured was 2 min, the time for the mice to explore the object was relatively short. On the other hand, we used 6-wk-old mice for the experiment and the behavioral tests were performed after 180 d, which possibly resulted in poor memory ability due to the older age of the mice.

One of the key features of neurodegenerative diseases is the death of neurons.[52] Our results suggested that exposure to PS-MPs induced higher levels in the expression levels of proapoptotic proteins in the hippocampus. In addition, the regulation of synaptic growth and plasticity also contributes to cognitive and learning and memory functions.[53,54] Changes in the density of dendritic spines after external stimulation can also lead to neurodegenerative diseases and intellectual disability.[55] In this study, mice exposed to PS-MPs had lower numbers of spines in the hippocampus. Meanwhile, synaptophysin is essential in maintaining homeostasis of memory function.[56,57] Our study suggested that the levels of synapsin 1, synaptophysin, and PSD 95 were lower in a concentration-dependent manner after PS-MPs treatment. Moreover, the results showed that the expression of *Syt 1* and *Bdnf*,[58,59] which are necessary for the regulation of neurodevelopment and synaptogenesis of hippocampal neurons, was lower following PS-MPs exposure.

To investigate whether the neurotoxicity of MPs was concentration dependent, we referred to some previous studies[5,32] and finally chose two concentrations, 100 and 1,000 μg/L, as experimental concentrations. In fact, the experimental concentrations we used (0.3 μg/d and 3 μg/d) were lower than those in some previous studies. Deng et al.[15] and Wang et al.[6] chose 0.1 mg/day to demonstrate the toxicity of mice. Hou et al. exposed mice to 0.6–0.7, 6–7, and 60–70 μg/d to explore reproductive toxicity of PS-MPs.[44] On the other hand, the particle size of MPs may be another vital factor affecting their toxicity and accumulation in different tissues according to some scholars.[60–62] Therefore, we chose three particle diameters to reveal the toxic impacts of PS-MPs on the nervous system of mice in this study. The results showed that there was a concentration-dependent increasing trend, but no particle size-dependent effect on the neurotoxicity of MPs.

Generally, the methods of detecting MPs accumulation in tissues include Raman spectroscopy,[63,64] polarized light microscopy,[65] and fluorescently labeled detection.[66] However, it is not possible to perfectly qualitatively and quantitatively detect MPs in tissues. In our study, to minimize the loss of MPs in tissue dissolution, we applied fluorescence imaging to detect the accumulation of PS-MPs in the whole brain without pretreatment.

Certainly, there are limitations in the present study. The PS-MPs used in this study were pristine MPs, which would therefore not represent MPs in nature that may have adsorbed other substances. Meanwhile, the method to detect the PS-MPs could not distinguish the different forms of the particle in tissues. Fluorescence imaging can only detect whether MPs can enter mouse brain tissue and cannot quantitatively detect the amount of MPs entering various parts of the brain tissue. In further study, we would explore more effective methods to detect whether PS-MPs enter the circulation and brain in a separated form or an aggregated form. We are eager to achieve further breakthroughs in detection technologies.

Conclusion

In summary, the effects of various exposure concentrations and particle sizes of PS-MPs exposure on the nervous system in mice were explored. Our studies suggest that chronic PS-MPs exposure disrupt the BBB, resulting in a lower density of dendritic spines, and higher mRNA levels of inflammation-related genes, bringing about memory impairment in mice. The outcomes measured here were concentration dependent, but independent of particle size. However, the limited experiments used to evaluate each outcome and the underlying mechanisms of PS-MPs–induced neurotoxicity and cognitive dysfunctions remain unclear, which will lead us to perform further studies.

Acknowledgments

This work was supported by the National Natural Science Foundation of China [31870492 (to H.X.), 31901182 (to D.L.), and 31971517], Natural Science Foundation of Jiangsu Province of China [BK20190316 (to J.D.)], and Fundamental Research Funds for the Central Universities [0214–14380438 (to J.D.) and 0214–14380471].

References

1. Katsnelson A. 2015. News feature: microplastics present pollution puzzle. Proc Natl Acad Sci USA 112(18):5547–5549, PMID: 25944930, https://doi.org/10.1073/pnas.1504135112.
2. Rochman CM, Browne MA, Halpern BS, Hentschel BT, Hoh E, Karapanagioti HK, et al. 2013. Policy: classify plastic waste as hazardous. Nature 494(7436):169–171, PMID: 23407523, https://doi.org/10.1038/494169a.
3. Cole M, Lindeque P, Fileman E, Halsband C, Goodhead R, Moger J, et al. 2013. Microplastic ingestion by zooplankton. Environ Sci Technol 47(12):6646–6655, PMID: 23692270, https://doi.org/10.1021/es400663f.
4. Ivar do Sul JA, Costa MF. 2014. The present and future of microplastic pollution in the marine environment. Environ Pollut 185:352–364, PMID: 24275078, https://doi.org/10.1016/j.envpol.2013.10.036.
5. Jin Y, Lu L, Tu W, Luo T, Fu Z. 2019. Impacts of polystyrene microplastic on the gut barrier, microbiota and metabolism of mice. Sci Total Environ 649:308–317, PMID: 30176444, https://doi.org/10.1016/j.scitotenv.2018.08.353.
6. Wang YL, Lee YH, Hsu YH, Chiu IJ, Huang CCY, Huang CC, et al. 2021. The kidney-related effects of polystyrene microplastics on human kidney proximal tubular epithelial cells HK-2 and male C57BL/6 mice. Environ Health Perspect 129(5):57003, PMID: 33956507, https://doi.org/10.1289/EHP7612.
7. Xie X, Deng T, Duan J, Xie J, Yuan J, Chen M. 2020. Exposure to polystyrene microplastics causes reproductive toxicity through oxidative stress and activation of the p38 MAPK signaling pathway. Ecotoxicol Environ Saf 190:110133, PMID: 31896473, https://doi.org/10.1016/j.ecoenv.2019.110133.
8. Araújo AP, Gomes AR, Malafaia G. 2020. Hepatotoxicity of pristine polyethylene microplastics in neotropical *Physalaemus cuvieri* tadpoles (Fitzinger, 1826). J Hazard Mater 386:121992, PMID: 31901713, https://doi.org/10.1016/j.jhazmat.2019.121992.
9. Lu Y, Zhang Y, Deng Y, Jiang W, Zhao Y, Geng J, et al. 2016. Uptake and accumulation of polystyrene microplastics in zebrafish (*Danio rerio*) and toxic effects in liver. Environ Sci Technol 50(7):4054–4060, PMID: 26950772, https://doi.org/10.1021/acs.est.6b00183.
10. Ding J, Zhang S, Razanajatovo RM, Zou H, Zhu W. 2018. Accumulation, tissue distribution, and biochemical effects of polystyrene microplastics in the freshwater fish red tilapia (*Oreochromis niloticus*). Environ Pollut 238:1–9, PMID: 29529477, https://doi.org/10.1016/j.envpol.2018.03.001.
11. Chen H, Hua X, Li H, Wang C, Dang Y, Ding P, et al. 2021. Transgenerational neurotoxicity of polystyrene microplastics induced by oxidative stress in *Caenorhabditis elegans*. Chemosphere 272:129642, PMID: 33465611, https://doi.org/10.1016/j.chemosphere.2021.129642.
12. Iheanacho SC, Odo GE. 2020. Neurotoxicity, oxidative stress biomarkers and haematological responses in African catfish (*Clarias gariepinus*) exposed to polyvinyl chloride microparticles. Comp Biochem Physiol C Toxicol Pharmacol 232:108741, PMID: 32171890, https://doi.org/10.1016/j.cbpc.2020.108741.
13. Chen Q, Gundlach M, Yang S, Jiang J, Velki M, Yin D, et al. 2017. Quantitative investigation of the mechanisms of microplastics and nanoplastics toward zebrafish larvae locomotor activity. Sci Total Environ 584–585:1022–1031, PMID: 28185727, https://doi.org/10.1016/j.scitotenv.2017.01.156.
14. Barboza LGA, Vieira LR, Branco V, Figueiredo N, Carvalho F, Carvalho C, et al. 2018. Microplastics cause neurotoxicity, oxidative damage and energy-related

changes and interact with the bioaccumulation of mercury in the European seabass, *Dicentrarchus labrax* (Linnaeus, 1758). Aquat Toxicol 195:49–57, PMID: 29287173, https://doi.org/10.1016/j.aquatox.2017.12.008.
15. Deng Y, Zhang Y, Lemos B, Ren H. 2017. Tissue accumulation of microplastics in mice and biomarker responses suggest widespread health risks of exposure. Sci Rep 7:46687, PMID: 28436478, https://doi.org/10.1038/srep46687.
16. Sarasamma S, Audira G, Siregar P, Malhotra N, Lai YH, Liang ST, et al. 2020. Nanoplastics cause neurobehavioral impairments, reproductive and oxidative damages, and biomarker responses in zebrafish: throwing up alarms of wide spread health risk of exposure. Int J Mol Sci 21(4):1410, PMID: 32093039, https://doi.org/10.3390/ijms21041410.
17. Deng W, Aimone JB, Gage FH. 2010. New neurons and new memories: how does adult hippocampal neurogenesis affect learning and memory? Nat Rev Neurosci 11(5):339–350, PMID: 20354534, https://doi.org/10.1038/nrn2822.
18. Nguyen PV, Abel T, Kandel ER, Bourtchouladze R. 2000. Strain-dependent differences in LTP and hippocampus-dependent memory in inbred mice. Learn Mem 7(3):170–179, PMID: 10837506, https://doi.org/10.1101/lm.7.3.170.
19. Kutlu MG, Gould TJ. 2016. Effects of drugs of abuse on hippocampal plasticity and hippocampus-dependent learning and memory: contributions to development and maintenance of addiction. Learn Mem 23(10):515–533, PMID: 27634143, https://doi.org/10.1101/lm.042192.116.
20. Kim EJ, Pellman B, Kim JJ. 2015. Stress effects on the hippocampus: a critical review. Learn Mem 22(9):411–416, PMID: 26286651, https://doi.org/10.1101/lm.037291.114.
21. Morris RGM. 1981. Spatial localization does not require the presence of local cues. Learn Motiv 12(2):239–260, https://doi.org/10.1016/0023-9690(81)90020-5.
22. Ennaceur A, Delacour J. 1988. A new one-trial test for neurobiological studies of memory in rats. I. behavioral data. Behav Brain Res 31(1):47–59, PMID: 3228475, https://doi.org/10.1016/0166-4328(88)90157-X.
23. Leger M, Quiedeville A, Bouet V, Haelewyn B, Boulouard M, Schumann-Bard P, et al. 2013. Object recognition test in mice. Nat Protoc 8(12):2531–2537, PMID: 24263092, https://doi.org/10.1038/nprot.2013.155.
24. Abbott NJ, Patabendige AA, Dolman DEM, Yusof SR, Begley DJ. 2010. Structure and function of the blood–brain barrier. Neurobiol Dis 37(1):13–25, PMID: 19664713, https://doi.org/10.1016/j.nbd.2009.07.030.
25. Abbott NJ. 2013. Blood–brain barrier structure and function and the challenges for CNS drug delivery. J Inherit Metab Dis 36(3):437–449, PMID: 23609350, https://doi.org/10.1007/s10545-013-9608-0.
26. Hawkins BT, Davis TP. 2005. The blood-brain barrier/neurovascular unit in health and disease. Pharmacol Rev 57(2):173–185, PMID: 15914466, https://doi.org/10.1124/pr.57.2.4.
27. Shou Y, Huang Y, Zhu X, Liu C, Hu Y, Wang H. 2019. A review of the possible associations between ambient PM2.5 exposures and the development of Alzheimer's disease. Ecotoxicol Environ Saf 174:344–352, PMID: 30849654, https://doi.org/10.1016/j.ecoenv.2019.02.086.
28. Liu X, Su P, Meng S, Aschner M, Cao Y, Luo W, et al. 2017. Role of matrix metalloproteinase-2/9 (MMP2/9) in lead-induced changes in an *in vitro* blood-brain barrier model. Int J Biol Sci 13(11):1351–1360, PMID: 29209140, https://doi.org/10.7150/ijbs.20670.
29. Iqubal A, Ahmed M, Ahmad S, Sahoo CR, Iqubal MK, Haque SE. 2020. Environmental neurotoxic pollutants: review. Environ Sci Pollut Res Int 27(33):41175–41198, PMID: 32820440, https://doi.org/10.1007/s11356-020-10539-z.
30. Branca JJV, Morucci G, Pacini A. 2018. Cadmium-induced neurotoxicity: still much ado. Neural Regen Res 13(11):1879–1882, PMID: 30233056, https://doi.org/10.4103/1673-5374.239434.
31. Wang J, Zhang C, Zhu J, Ding J, Chen Y, Han X. 2019. Blood-brain barrier disruption and inflammation reaction in mice after chronic exposure to Microcystin-LR. Sci Total Environ 689:662–678, PMID: 31279213, https://doi.org/10.1016/j.scitotenv.2019.06.387.
32. Lu L, Wan Z, Luo T, Fu Z, Jin Y. 2018. Polystyrene microplastics induce gut microbiota dysbiosis and hepatic lipid metabolism disorder in mice. Sci Total Environ 631–632:449–458, PMID: 29529433, https://doi.org/10.1016/j.scitotenv.2018.03.051.
33. Eerkes-Medrano D, Thompson RC, Aldridge DC. 2015. Microplastics in freshwater systems: a review of the emerging threats, identification of knowledge gaps and prioritisation of research needs. Water Res 75:63–82, PMID: 25746963, https://doi.org/10.1016/j.watres.2015.02.012.
34. Peng G, Xu P, Zhu B, Bai M, Li D. 2018. Microplastics in freshwater river sediments in Shanghai, China: a case study of risk assessment in mega-cities. Environ Pollut 234:448–456, PMID: 29207296, https://doi.org/10.1016/j.envpol.2017.11.034.
35. Jin H, Yan M, Pan C, Liu Z, Sha X, Jiang C, et al. 2022. Chronic exposure to polystyrene microplastics induced male reproductive toxicity and decreased testosterone levels via the LH-mediated LHR/cAMP/PKA/StAR pathway. Part Fibre Toxicol 19(1):13, PMID: 35177090, https://doi.org/10.1186/s12989-022-00453-2.
36. Schneider CA, Rasband WS, Eliceiri KW. 2012. NIH image to ImageJ: 25 years of image analysis. Nat Methods 9(7):671–675, PMID: 22930834, https://doi.org/10.1038/nmeth.2089.
37. Livak KJ, Schmittgen TD. 2001. Analysis of relative gene expression data using real-time quantitative PCR and the $2^{-\Delta\Delta C(T)}$ method. Methods 25(4):402–408, PMID: 11846609, https://doi.org/10.1006/meth.2001.1262.
38. Sørensen KK, Simon-Santamaria J, McCuskey RS, Smedsrød B. 2015. Liver sinusoidal endothelial cells. Compr Physiol 5(4):1751–1774, PMID: 26426467, https://doi.org/10.1002/cphy.c140078.
39. Barnes DKA, Galgani F, Thompson RC, Barlaz M. 2009. Accumulation and fragmentation of plastic debris in global environments. Philos Trans R Soc Lond B Biol Sci 364(1526):1985–1998, PMID: 19528051, https://doi.org/10.1098/rstb.2008.0205.
40. Jambeck JR, Geyer R, Wilcox C, Siegler TR, Perryman M, Andrady A, et al. 2015. Marine pollution. Plastic waste inputs from land into the ocean. Science 347(6223):768–771, PMID: 25678662, https://doi.org/10.1126/science.1260352.
41. Phillips MB, Bonner TH. 2015. Occurrence and amount of microplastic ingested by fishes in watersheds of the Gulf of Mexico. Mar Pollut Bull 100(1):264–269, PMID: 26388444, https://doi.org/10.1016/j.marpolbul.2015.08.041.
42. Dong CD, Chen CW, Chen YC, Chen HH, Lee JS, Lin CH. 2020. Polystyrene microplastic particles: *in vitro* pulmonary toxicity assessment. J Hazard Mater 385:121575, PMID: 31727530, https://doi.org/10.1016/j.jhazmat.2019.121575.
43. Amereh F, Babaei M, Eslami A, Fazelipour S, Rafiee M. 2020. The emerging risk of exposure to nano(micro)plastics on endocrine disturbance and reproductive toxicity: from a hypothetical scenario to a global public health challenge. Environ Pollut 261:114158, PMID: 32088433, https://doi.org/10.1016/j.envpol.2020.114158.
44. Hou B, Wang F, Liu T, Wang Z. 2021. Reproductive toxicity of polystyrene microplastics: in vivo experimental study on testicular toxicity in mice. J Hazard Mater 405:124028, PMID: 33087287, https://doi.org/10.1016/j.jhazmat.2020.124028.
45. Tang Y, Zhou W, Sun S, Du X, Han Y, Shi W, et al. 2020. Immunotoxicity and neurotoxicity of bisphenol A and microplastics alone or in combination to a bivalve species, *Tegillarca granosa*. Environ Pollut 265(pt A):115115, PMID: 32806413, https://doi.org/10.1016/j.envpol.2020.115115.
46. Sun T, Zhan J, Li F, Ji C, Wu H. 2021. Environmentally relevant concentrations of microplastics influence the locomotor activity of aquatic biota. J Hazard Mater 414:125581, PMID: 34030420, https://doi.org/10.1016/j.jhazmat.2021.125581.
47. Chow BW, Gu C. 2015. The molecular constituents of the blood–brain barrier. Trends Neurosci 38(10):598–608, PMID: 26442694, https://doi.org/10.1016/j.tins.2015.08.003.
48. Obermeier B, Daneman R, Ransohoff RM. 2013. Development, maintenance and disruption of the blood-brain barrier. Nat Med 19(12):1584–1596, PMID: 24309662, https://doi.org/10.1038/nm.3407.
49. AlFadly ED, Elzahhar PA, Tramarin A, Elkazaz S, Shaltout H, Abu-Serie MM, et al. 2019. Tackling neuroinflammation and cholinergic deficit in Alzheimer's disease: multi-target inhibitors of cholinesterases, cyclooxygenase-2 and 15-lipoxygenase. Eur J Med Chem 167:161–186, PMID: 30771604, https://doi.org/10.1016/j.ejmech.2019.02.012.
50. Barnhart CD, Yang D, Lein PJ. 2015. Using the Morris water maze to assess spatial learning and memory in weanling mice. PLoS One 10(4):e0124521, PMID: 25886563, https://doi.org/10.1371/journal.pone.0124521.
51. Lueptow LM. 2017. Novel object recognition test for the investigation of learning and memory in mice. J Vis Exp 126:55718, PMID: 28892027, https://doi.org/10.3791/55718.
52. Ahmed MR, Shaikh MA, Ul Haq SHI, Nazir S. 2018. Neuroprotective role of chrysin in attenuating loss of dopaminergic neurons and improving motor, learning and memory functions in rats. Int J Health Sci (Qassim) 12(3):35–43, PMID: 29896070.
53. Segal M. 2017. Dendritic spines: morphological building blocks of memory. Neurobiol Learn Mem 138:3–9, PMID: 27311757, https://doi.org/10.1016/j.nlm.2016.06.007.
54. Mahmmoud RR, Sase S, Aher YD, Sase A, Gröger M, Mokhtar M, et al. 2015. Spatial and working memory is linked to spine density and mushroom spines. PLoS One 10(10):e0139739, PMID: 26469788, https://doi.org/10.1371/journal.pone.0139739.
55. Maiti P, Manna J, Ilavazhagan G, Rossignol J, Dunbar GL. 2015. Molecular regulation of dendritic spine dynamics and their potential impact on synaptic plasticity and neurological diseases. Neurosci Biobehav Rev 59:208–237, PMID: 26562682, https://doi.org/10.1016/j.neubiorev.2015.09.020.
56. Harper CB, Mancini GMS, van Slegtenhorst M, Cousin MA. 2017. Altered synaptobrevin-II trafficking in neurons expressing a synaptophysin mutation associated with a severe neurodevelopmental disorder. Neurobiol Dis 108:298–306, PMID: 28887151, https://doi.org/10.1016/j.nbd.2017.08.021.

57. Miranda AM, Herman M, Cheng R, Nahmani E, Barrett G, Micevska E, et al. 2018. Excess synaptojanin 1 contributes to place cell dysfunction and memory deficits in the aging hippocampus in three types of Alzheimer's disease. Cell Rep 23(10):2967–2975, PMID: 29874583, https://doi.org/10.1016/j.celrep.2018.05.011.
58. Choi SH, Bylykbashi E, Chatila ZK, Lee SW, Pulli B, Clemenson GD, et al. 2018. Combined adult neurogenesis and BDNF mimic exercise effects on cognition in an Alzheimer's mouse model. Science 361(6406):eaan8821, PMID: 30190379, https://doi.org/10.1126/science.aan8821.
59. Oh H, Piantadosi SC, Rocco BR, Lewis DA, Watkins SC, Sibille E. 2019. The role of dendritic brain-derived neurotrophic factor transcripts on altered inhibitory circuitry in depression. Biol Psychiatry 85(6):517–526, PMID: 30449530, https://doi.org/10.1016/j.biopsych.2018.09.026.
60. Wright SL, Thompson RC, Galloway TS. 2013. The physical impacts of microplastics on marine organisms: a review. Environ Pollut 178:483–492, PMID: 23545014, https://doi.org/10.1016/j.envpol.2013.02.031.
61. Browne MA, Dissanayake A, Galloway TS, Lowe DM, Thompson RC. 2008. Ingested microscopic plastic translocates to the circulatory system of the mussel, *Mytilus edulis* (L). Environ Sci Technol 42(13):5026–5031, PMID: 18678044, https://doi.org/10.1021/es800249a.
62. Hämer J, Gutow L, Köhler A, Saborowski R. 2014. Fate of microplastics in the marine isopod *Idotea emarginata*. Environ Sci Technol 48(22):13451–13458, PMID: 25289587, https://doi.org/10.1021/es501385y.
63. Qiao R, Deng Y, Zhang S, Wolosker MB, Zhu Q, Ren H, et al. 2019. Accumulation of different shapes of microplastics initiates intestinal injury and gut microbiota dysbiosis in the gut of zebrafish. Chemosphere 236:124334, PMID: 31310986, https://doi.org/10.1016/j.chemosphere.2019.07.065.
64. Oßmann BE, Sarau G, Schmitt SW, Holtmannspötter H, Christiansen SH, Dicke W. 2017. Development of an optimal filter substrate for the identification of small microplastic particles in food by micro-Raman spectroscopy. Anal Bioanal Chem 409(16):4099–4109, PMID: 28439620, https://doi.org/10.1007/s00216-017-0358-y.
65. Karami A, Groman DB, Wilson SP, Ismail P, Neela VK. 2017. Biomarker responses in zebrafish (*Danio rerio*) larvae exposed to pristine low-density polyethylene fragments. Environ Pollut 223:466–475, PMID: 28129952, https://doi.org/10.1016/j.envpol.2017.01.047.
66. Lee KW, Shim WJ, Kwon OY, Kang JH. 2013. Size-dependent effects of micro polystyrene particles in the marine copepod *Tigriopus japonicus*. Environ Sci Technol 47(19):11278–11283, PMID: 23988225, https://doi.org/10.1021/es401932b.